

Valley transport in Kekulé structures of graphene

Juan-Juan Wang(王娟娟) and Jun Wang(汪军)
Citation: Chin. Phys. B, 2024, 33 (**1**): 017801. DOI: 10.1088/1674-1056/acf9e3
Journal homepage: http://cpb.iphy.ac.cn; http://iopscience.iop.org/cpb

What follows is a list of articles you may be interested in

Temperature-dependent photoluminescence of lead-free cesium tin halide perovskite microplates

Jiayu Tan(谭佳雨), Yixuan Zhou(周译玄), De Lu(卢德), Xukun Feng(冯旭坤), Yuqi Liu(刘玉琪), Mengen Zhang(张蒙恩), Fangzhengyi Lu(卢方正一), Yuanyuan Huang(黄媛媛), and Xinlong Xu(徐新龙)
Chin. Phys. B, 2023, 32 (**11**): 117802. DOI: 10.1088/1674-1056/ad028e

Probing photocarrier dynamics of pressurized graphene using time-resolved terahertz spectroscopy

Yunfeng Wang(王云峰), Shujuan Xu(许淑娟), Jin Yang(杨金), and Fuhai Su(苏付海)
Chin. Phys. B, 2023, 32 (**6**): 067802. DOI: 10.1088/1674-1056/acc2b1

Graphene metasurface-based switchable terahertz half-/quarter-wave plate with a broad bandwidth

Xiaoqing Luo(罗小青), Juan Luo(罗娟), Fangrong Hu(胡放荣), and Guangyuan Li(李光元)
Chin. Phys. B, 2023, 32 (**2**): 027801. DOI: 10.1088/1674-1056/ac80a8

Dual-channel tunable near-infrared absorption enhancement with graphene induced by coupled modes of topological interface states

Zeng-Ping Su(苏增平), Tong-Tong Wei(魏彤彤), and Yue-Ke Wang(王跃科)
Chin. Phys. B, 2022, 31 (**8**): 087804. DOI: 10.1088/1674-1056/ac6744

Faraday rotations, ellipticity, and circular dichroism in magneto-optical spectrum of moiré superlattices

J A Crosse and Pilkyung Moon
Chin. Phys. B, 2021, 30 (**7**): 077803. DOI: 10.1088/1674-1056/ac051f

---

TOPICAL REVIEW — Valleytronics

Valley transport in Kekulé structures of graphene

Juan-Juan Wang(王娟娟)[1,†] and Jun Wang(汪军)[2,‡]

[1] *Department of Physics, College of Sciences, Nanjing Agricultural University, Nanjing* 210095, *China*
[2] *Department of Physics, Southeast University, Nanjing* 210096, *China*

(Received 22 June 2023; revised manuscript received 4 September 2023; accepted manuscript online 15 September 2023)

Valleytronics is an emergent discipline in condensed matter physics and offers a new way to encode and manipulate information based on the valley degree of freedom in materials. Among the various materials being studied, Kekulé distorted graphene has emerged as a promising material for valleytronics applications. Graphene can be artificially distorted to form the Kekulé structures rendering the valley-related interaction. In this work, we review the recent progress of research on Kekulé structures of graphene and focus on the modified electronic bands due to different Kekulé distortions as well as their effects on the transport properties of electrons. We systematically discuss how the valley-related interaction in the Kekulé structures was used to control and affect the valley transport including the valley generation, manipulation, and detection. This article summarizes the current challenges and prospects for further research on Kekulé distorted graphene and its potential applications in valleytronics.

Keywords: graphene, Y-shaped Kekulé (Y-Kek) lattice distortion structure, O-Kekulé (O-Kek) structure, valley current

PACS: 78.20.Jq, 71.70.Fk, 72.80.Vp **DOI:** 10.1088/1674-1056/acf9e3

1. Introduction

The electronic properties of graphene at low energy are governed by the Dirac particle characteristics due to its hexagonal honeycomb lattice structure. Meanwhile, the Dirac electrons have additional lattice pseudospin and valley degrees of freedom besides the conventional charge and spin degrees of freedom.[1–4] Compared to the charge degree of freedom, the valley degree of freedom has lower power consumption and faster data processing speed in carrying and storing information[5,6] when it is used as a degree of freedom to make a new generation of electronic devices.

Currently, researches on the valley degree of freedom of Dirac electrons are expanded from graphene materials to other two-dimensional honeycomb structural materials,[7–18] such as silicene,[7] MoS_2,[8–12] etc. A vast amount of methods were shown to effectively generate, manipulate, and detect the valley pseudospin.[2,3,19–26] For examples, Milovanovic *et al.*[20] showed that the pseudomagnetic field generated by the strain protrusions with certain height and width can produce valley-polarized currents in a multi-terminal graphene device. Yao *et al.*[26] found that the propagation direction of Dirac electrons in graphene line-defect lattice structures is locked with the valley degree of freedom under the action of the pseudomagnetic field owing to the nonuniform strains, and this can generate the valley-polarized currents simultaneously.

By inducing the Kekulé distortion[27–31] or special atom-adsorption potentials[32,33] in the graphene lattice to produce a superlattice structure with a primitive cell enlarged three times than that of the original one,[14,15,30,31] the two valleys could be folded together in the system. So the coupling of the two valleys has been extensively investigated to control the valley degree of freedom in literature.[30–39]

In 2016, Gutierrez *et al.*[36] through experiment found that when graphene thin films were epitaxially grown on a Cu substrate, Cu atom vacancy was present in every six carbon atoms, and the unit cell of the structure was enlarged three times than that of the pristine graphene one. Consequently, the lattice hopping energy between the carbon atom with the Cu atom vacancy and its adjacent three carbon atoms is uniformly modified,[36,40,41] and a periodic superlattice structure forms. This structure is called the Y-shaped Kekulé lattice distortion (Y-Kek)[36] as shown in Fig. 1(a). The two valleys of the Dirac electrons in the Y-Kek structure are no longer degenerate,[40,42] and the valley–momentum locking effect occurs.[40] The energy dispersion is the interlocking of two Dirac cones with different Fermi velocities,[40,43] exhibiting valley-dependent linear dispersion relationship.[30,36,40] In addition, there is another type of Kekulé distorted superlattice structure as shown in Fig. 1(b) termed as the O-Kekulé structure (O-Kek),[31,40,41,44] where the hopping energies of every next-nearest neighboring bonds within every six carbon atoms are modified. In the O-Kek structure, an energy gap is opened at the Dirac point,[31,40,41,45,46] and the two helical valleys are degenerate.[31,40,41,45,46] The structure is now a valley-version topological insulator causing significant variation of the band

†Corresponding author. E-mail: juanjuanwang@njau.edu.cn
‡Corresponding author. E-mail: jwang@seu.edu.cn

© 2024 Chinese Physical Society and IOP Publishing Ltd

structure. Both two types of Kekulé superlattice structures fold the K and K' points of the original graphene into the center of the Brillouin zone (Γ) as shown in Fig. 1(c).[30,31,40,41]

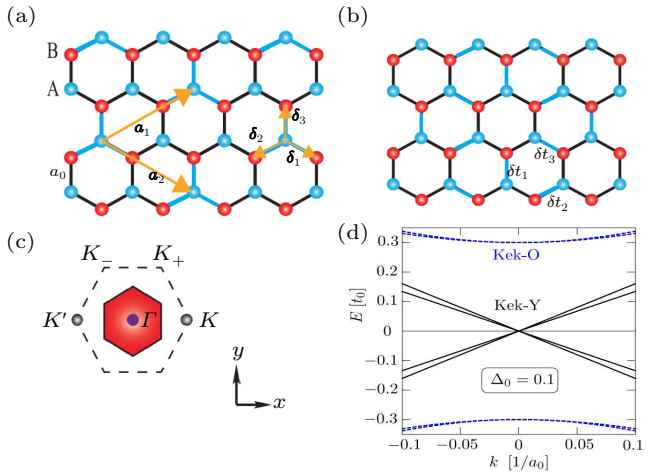


Fig. 1. Schematic diagram of (a) Y-Kek and (b) O-Kek distorted graphene superlattice structures. The blue solid lines represent the contraction of the three carbon–carbon bond lengths in the supercell. $\boldsymbol{\delta}_i$ $(i = 1,2,3)$ are the nearest-neighbor carbon atom vectors. δt_i $(i = 1,2,3)$ refer to the electronic hopping energy correction terms between carbon atoms caused by the contraction of carbon–carbon bond lengths in the Kekulé structure. (c) The Brillouin zone of the original graphene and Y-Kek (O-Kek) structures overlaps at the center point Γ for the K and K' valleys (gray Dirac points). (d) Dispersion relations of the O-Kek (blue dashed line) and Y-Kek (black solid line) distorted graphene superlattice structures near the center of the Brillouin zone. Panel (d) is reproduced from Ref. [40]. ©2018 The Author(s). Published by IOP Publishing Ltd on behalf of Deutsche Physikalische Gesellschaft. All rights reserved.

In recent years, the study of valleytronics in Kekulé graphene structures has successfully attracted widespread attention due to its unique valley-coupling effect in the system,[40] which can be used to control the valley transport.[30,31,47–55] In 2021, Bao *et al.*[44] inserted Li[56] atoms between graphene sheets and SiC substrate realizing a Kekulé superlattice structure, and confirmed the breaking of valley chirality symmetry in Kekulé structure[30,31,36,41,50] as well as the generation of a topological phase with valley–orbit coupling.[50]

Currently, it has been proposed that the valley-related interaction in the Kekulé structures,[36,44,50] especially the one breaking valley chiral symmetry, can lead to numerous interesting transport properties of valley electrons.[30,31,50] Santacruz *et al.*[57] found that valley–momentum coupling in the Y-Kek structure can result in a low attenuation rate and low frequency valley-driven oscillatory motion of the wave packets of Dirac electrons. The theoretical research by Beenakker *et al.*[40] showed that the Y-Kek graphene can induce valley isospin locking with momentum direction in a parallel or antiparallel configuration. The mirror-symmetric Y-Kek structure has two chiral valleys, which still possess the massless properties of Dirac fermions. This can lead to the disappearance of the valley degeneracy of Landau levels related to the magnetic field. The coupling of valley and momentum[40] can lead to the emergence of many novel physical properties in the Kekulé structures, such as valley precession,[30] the enhanced Andreev reflection,[47] and the valley supercurrent,[31] integer quantum Hall effect,[58] and supercurrent rectification effect.[59]

In this work, we mainly review some recent progresses of valley transport in two-dimensional Kekulé graphene superlattices. In Section 2, we briefly introduce the characteristics of the Kekulé structures as well as the modified energy band. In Section 3, we discuss the researches of the generation of valley current in Kekulé structures. In Section 4, we introduce some proposed methods to manipulate the valley current flowing in Kekulé structures. In Section 5, we review the works about the detection of valley current in Kekulé structures. We summarize the current challenges and issues of the valleytronics research on Kekulé structures in the last section.

2. Characteristics of the Kekulé structures

We first introduce the characteristics of the Kekulé-distorted lattice structure and the resulting energy band structure. As schematically shown in Figs. 1(a) and 1(b), the Kekulé distorted graphene is based on the original hexagonal honeycomb lattice while the lattice vectors are given by[40]

$$\boldsymbol{a}_1 = \frac{a_0}{2}(3\sqrt{3}, 3), \tag{1}$$

$$\boldsymbol{a}_2 = \frac{a_0}{2}(3\sqrt{3}, -3). \tag{2}$$

Here, a_0 is the nearest neighbor spacing of carbon atoms in the original graphene lattice.[40,60] In real space, the three nearest neighbor vectors are given by $\boldsymbol{\delta}_1 = \frac{1}{2}(\sqrt{3}, -1), \boldsymbol{\delta}_2 = -\frac{1}{2}(\sqrt{3}, 1), \boldsymbol{\delta}_3 = (0, 1)$. A (blue dot) and B (red dot) are used to mark the two non-equivalent carbon atoms in each primitive cell. As shown in Fig. 1(c), the two original K and K' valleys in the reciprocal lattice space are distributed at two vertices of the Brillouin region of graphene but now for the Kekulé structure, the K valley and K' valley are located respectively in the new reciprocal lattice sites as[40] $\boldsymbol{K}_\pm = \frac{2}{9}\pi\sqrt{3}(\pm 1, \sqrt{3})$.

The Hamiltonian of the Kekulé lattice tight-binding model can be expressed as[40]

$$H = -\Sigma_{\boldsymbol{r}}\Sigma_{j=1}^{3} t_{\boldsymbol{r},j} a_{\boldsymbol{r}}^{\dagger} b_{\boldsymbol{r}+\boldsymbol{\delta}_j} + \text{h.c.} \tag{3}$$

The creation operator of the A carbon atom at the spatial coordinate $\boldsymbol{r}$ is represented by $a_{\boldsymbol{r}}^{\dagger}$, while the annihilation operator of the B carbon atom at the spatial coordinate $\boldsymbol{r} + \boldsymbol{\delta}_j$ is represented by $b_{\boldsymbol{r}+\boldsymbol{\delta}_j}$. The hopping energy between the A carbon atom at the spatial coordinate $\boldsymbol{r}$ and its three nearest neighboring B carbon atoms reads[40]

$$t_{r,j} = t_0\{1 + 2\text{Re}[\Delta\, \text{e}^{\text{i}(p\boldsymbol{K}_+ + q\boldsymbol{K}_-)\cdot\boldsymbol{\delta}_j + \text{i}\frac{2\pi n}{3}}]\},$$
$$p, q \in Z,\ \ n \in Z, \tag{4}$$

where t_0 represents the hopping energy between the nearest neighboring carbon atoms in the original graphene structure.

$\Delta = \Delta_0 e^{i\phi}$ represents the coupling term between the K and K' valleys caused by lattice distortion.[30,31,40,61] It is not difficult to obtain the energy dispersion of both types of Kekulé structures and they are given by[40,46]

$$E_{\text{O-Kek}} = \sqrt{v_f^2|\boldsymbol{k}|^2 + (3t_0\Delta_0)^2}, \tag{5}$$

$$E_{\text{Y-Kek}} = v_f(1+\Delta_0)|\boldsymbol{k}|. \tag{6}$$

Here, v_f represents the Fermi velocity and $\boldsymbol{k}$ is the momentum extended from the K or K' point. It is seen that the energy dispersion of the Y-Kek structure has two split linear E–k while the O-Kek shows an energy gap opened at the band center as shown in Fig. 1(d). The energy gap is created by the valley coupling term and the magnitude is determined by the strength Δ_0.

In 2022, Garcia *et al.*[50] studied a generalized Hamiltonian of the Kekulé-distorted graphene by considering different hopping-energy and site-energy modifications, and they predicted various semimetal, metal, and topological insulator phases emergent in the Kekulé-graphene lattice. Figures 2(a) and 2(b) are the typical (semi) metallic phases, which are even more interesting by themselves since the two chiral valley bands can shift to each other within peculiar parameters. Figures 2(b)–2(h) are the several topological phases and the most intriguing aspect is that one of the valley bands is in a semimetallic phase while the other one is in a topological insulating phase. Gutierrez *et al.*[36] successfully fabricated the Y-Kek graphene lattice with the typical band structure as shown in Fig. 2(a) in the experiment. Afterwards, Eom *et al.*[62] confirmed the Kekulé topological phase with broken chiral symmetry of a single valley by using scanning tunneling microscopy, i.e., one band remains linear dispersion but the other opens a gap as shown in Fig. 2(c). Bao *et al.*[44] demonstrated the valley–orbit coupling topological phase shown in Fig. 2(f) by embedding Li[56] into double-layer graphene on a SiC substrate.

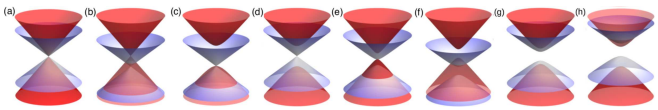


Fig. 2. (a)–(h) Topological phase diagram of the Kekulé structures, where red and blue represent the K_+ ($\nu = 1$) and K_- ($\nu = -1$) valleys, respectively. Massless Dirac fermions in both valleys with (a) $\mu_\nu = 0$, $\Delta\xi = \xi_+ - \xi_- = 0$ and (b) $\mu_\nu = 0$, $\Delta\xi = \xi_+ - \xi_- = 0.4$. Chiral symmetry breaking in a single valley with massless (c) $\mu_- = 0$, $\Delta\xi = 0.2$ and (d) massive $\mu_+ = -0.2$, $\Delta\xi = 0$ Dirac fermions. (e) Quadratic band crossing point with $\mu_- = -0.1$, $\mu_+ = -0.1$, $\Delta\xi = 0.2$. (f) Valley–orbit coupling with $\mu_- = 0.1$, $\mu_+ = -0.1$, $\Delta\xi = 0.4$. (g) Zeeman-like effect with $\mu_- = 0.15$, $\mu_+ = 0.25$, $\Delta\xi = 0$. (h) Crossing of conduction bands with $\mu_- = 0.2$, $\mu_+ = 0.3$, $\Delta\xi = -0.2$. ξ_ν and μ_ν are related to site energy modifications of the Kekulé structures. Panels (a)–(h) are reprinted figures with permission from Ref. [50]. Copyright ©2022 by the American Physical Society.

Therefore, the Kekulé-distorted graphene has various band structures including both the metallic/semimetallic and the topological insulating phases, which are very dependent on the different site-energy distributions as well as the different bond-energy configurations. In the following, we will introduce some characteristics of the valley transport affected by the Kekulé distortion in graphene.

3. Valley generation in Kekulé-distorted graphene

The valley coupling effect in the Kekulé structures can be employed to produce the valley polarized current. As the single valley case is shown in Fig. 2(c), the valley polarization can be obtained simply using a gate voltage. In 2014, Wang *et al.*[63] studied a time-dependent lattice distortion (TLD) of the O-Kek structure to produce pure valley current. The system Hamiltonian reads[61,63]

$$H(t) = \hbar v_F\left[(\sigma_x k_x + \sigma_y k_y)\eta_z + \boldsymbol{A}(t)\frac{\eta_x + i\eta_y}{2} + \boldsymbol{A}^*(t)\frac{\eta_x - i\eta_y}{2}\right], \tag{7}$$

where ω is the frequency, v_F is the Fermi velocity, the Pauli operator σ and η denote the A and B sublattice space and valley space, respectively. $\boldsymbol{A}(t) = (A_x + iA_y)e^{i\omega t} = Ae^{i(\omega t+\varphi)}$ is the gauge field induced by the time-varying Kekulé lattice vibration (distortion) of the optical phonon mode[61,63–65] with A being the distortion strength. The valley resonance effect and valley flow can be generated in this system.

Authors verified that the pure valley current can be pumped out from the time-dependent Kekulé region to the left/right graphene lead where the valley is well defined as schematically shown in Fig. 3(a). The K (K')-valley electrons are transported into the middle region below the Fermi energy and experience a valley flip by absorbing a photon so that a pure valley current forms. The process is actually a topological valley-version pump similar to the Thouless pump. Such a pure valley current can be reflected as the transverse voltage by the inverse valley Hall effect[66] in the circuit presented in Fig. 3(b). In Figs. 3(c) and 3(d), the reflection coefficient ($|r_{+-}|^2$) is a unit in the energy gap representing that a clear valley resonance effect appears and the quantized valley current pumps out the system when the frequency is in the energy gap, i.e., the time-dependent lattice distortion can generate a quantized valley current in O-Kek structure. Meanwhile, other optical and electrical pumping methods have also been employed to induce the valley polarized current in the similar graphene-like materials.[9,13] For example, Wang *et al.*[9] proposed that the valley and spin polarized currents can be generated and manipulated through an adiabatic electron pumping in single-layer MoS_2 since the valence band of material is valley–spin polarized.

Beenakker *et al.*[53] realized that the O-Kek structure has an energy gap as shown in Fig. 1(d) due to the introduction

of the valley coupling, so it resembles a superconductor due to the valley condensation like the usual charge condensation. The pairing was still between the K and K' valleys. They proposed a graphene/O-Kek superlattice hybrid junction and showed that there exists a valley flip effect at the interface of the junction, which is the same as the local Andreev reflection occurring in the usual metal/superconductor junction.[67] The K and K' valleys corresponded to the roles of electrons and holes in topological superconductors.

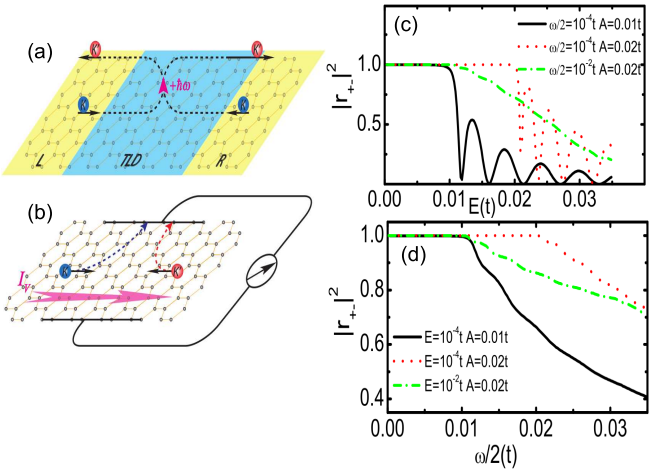


Fig. 3. (a) A diagram showing a device that resonates with two-terminal electron valleys. The time-dependent Kekulé distortion region generates pure valley currents made up of the oppositely moving K-valley and K'-valley electrons, which then flow into the left and right graphene leads. (b) Schematic of an electron valley detection device. As a result of the inverse valley Hall effect, a measurable transverse voltage is generated when the pumped valley current I_v is injected into a gapped graphene. Energy-averaged reflection coefficient $|r_{+-}|^2$ as a function of the (c) Fermi energy E and (d) TLD frequency ω. The unit reflection coefficients represent the quantized pump and A is the energy gap magnitude of the TLD region. Panels (a)–(d) are reprinted figures with permission from Ref. [63]. Copyright ©2014 by the American Physical Society.

In Figs. 4(a) and 4(b), authors found that the incident electrons in the K valley are completely reflected as K' electrons when the incident angle is approximately normal ($|q| < q_c$, q_c being the critical momentum) to the interface. Due to the topological phase transition, there is a transition from complete inter-valley reflection to complete intra-valley reflection at $q = \pm q_c$, ($v_F q_c = \sqrt{|\alpha|^2 - \mu^2}$, the parameters μ (real), α, and β (complex) are determined by the substrate potentials on these six atoms[53,68]). As shown in Fig. 4(a), q_c is a pair of conical points formed by the splitting of the Dirac cone due to the valley coupling. The valley flip process is protected by topological invariants and the complete reflection between the two valley electrons still occurs even with a large Fermi energy mismatch at the interface of the superlattice.[67]

By taking the O-Kek structure as a valley-condensed superconductor, Wang *et al.*[31] studied a hybrid junction of O-Kek/graphene/O-Kek heterostructure (GS/G/GS) shown in Fig. 5(a) that can be viewed as a Josephson-like junction to produce the valley supercurrent flowing in the system. In the O-Kek structure, the valley coupling term $\Delta e^{i\phi_j}$ ($j = L/R$) representing the left and right Kekulé structures is a complex number varying with the crystal axis or lattice distortion mode,[61,63] as a result, the valley coupling can have a different azimuthal phase same as the microscopic superconducting phase.

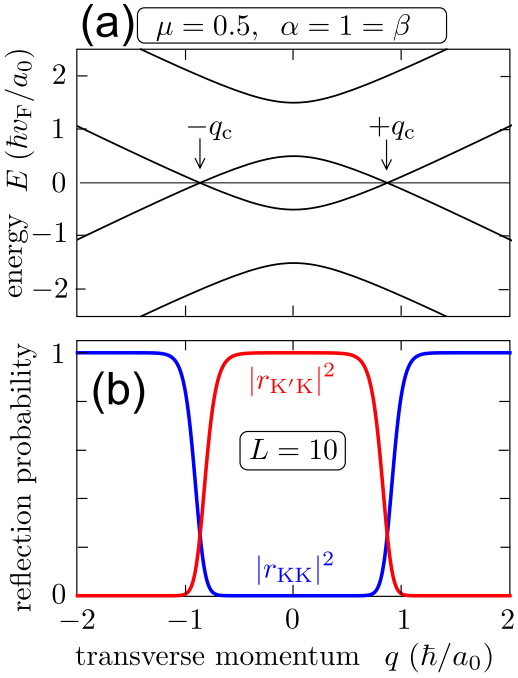


Fig. 4. (a) Energy spectrum of superlattice graphene. (b) Reflection probability $|r_{K'K(KK)}|^2$ as a function of the transverse momentum q. When a superlattice graphene strip with a length of $L = 10a_0$ is connected to heavily doped pristine-graphene electrodes at $x = 0$ and $x = L$ in the x-direction, the corresponding reflection probability shows complete reflection into the opposite valley in the topologically nontrivial regime near normal incidence ($|q| < q_c = \sqrt{|\alpha|^2 - \mu^2}$). Panels (a) and (b) are reprinted figures with permission from Ref. [53]. Copyright ©2018 by the American Physical Society.

In Fig. 5(b), authors show that the system has a spontaneous valley supercurrent flowing in the middle region where the valley is well defined without any Kekulé distortion. There are some different properties of valley supercurrents from the usual charge supercurrent. The global chemical potential μ can reverse the supercurrent when it moves away from the band center ($E = 0$) as shown in Fig. 5(d). While μ is less than the energy gap Δ, the discrete Andreev bound states in the energy gap significantly dominate the valley supercurrent J_v in comparison to the continuous states contributing to the valley current J_v in Fig. 5(c). The local potential applied on the junction can similarly induce the so-called 0–π state transition of the Josephson junction in Fig. 5(e). Certainly, there is no factor breaking time-reversal symmetry and thus, it is different from the conventional Josephson junction.

Garcia *et al.*[50] studied a Kekulé-distorted graphene pn junction schematically shown in Fig. 6(a), where the Dirac band can be modified specifically via different on-site and bond-energy modifications as shown in Fig. 2. So the valley-dependent transports are very abundant and various phenom-

ena exist like Klein tunneling, valley flip, valley fully polarization, and perfect valley filtering. The Klein-tunneling is shown in Fig. 6(b) while other panels display different valley-related transmissions and reflections in Figs. 6(c)–6(g). For example, the single valley (full valley polarization) transport represented by the red energy region is shown in Figs. 6(c)–6(g). The phenomenon of zero transmission of valley current can be achieved as shown in Figs. 6(f) and 6(g). According to these results, different valley-control devices for Kekulé-graphene heterostructures can be designed by selecting different parameters based on the corresponding topological phases of the Kekulé structures.

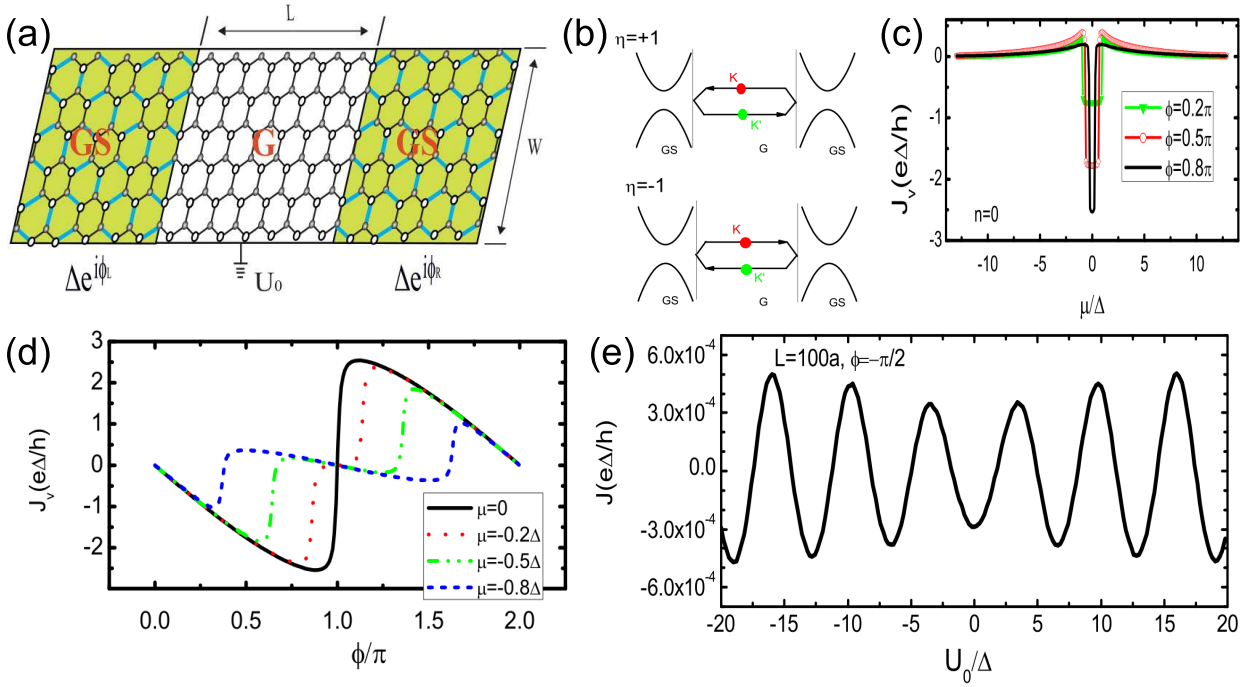


Fig. 5. (a) A GS/G/GS junction. $\Delta e^{i\phi_j}$ $(j = \mathrm{L,R})$ is valley coupling terms of the left and right O-Kek structures. An energy gap of the O-Kek structure depends on the magnitude of the term Δ. U_0 represents the gate voltage applied to the pristine graphene. L and W are the length and width of the junction, respectively. (b) Schematic of a self-closed path of quasiparticles reflected on the G/GS interfaces, where $\eta = \pm 1$ represents two opposite chiralities. Valley supercurrent J_v as a function of (c) the chemical potential μ with $W = 10000a$ and (d) phase ϕ with $|\mu| < \Delta$. (c) and (d) Other parameters are $k_y = 0$, $U_0 = 0$, and $L = 20a$. (e) The valley supercurrent density J as a function of the local potential U_0 with $\mu = 0$ and $W = 10000a$, a is the lattice constant. Panels (a)–(e) are reprinted from Ref. [31]. ©2020 The Authors. Published by the American Physical Society.

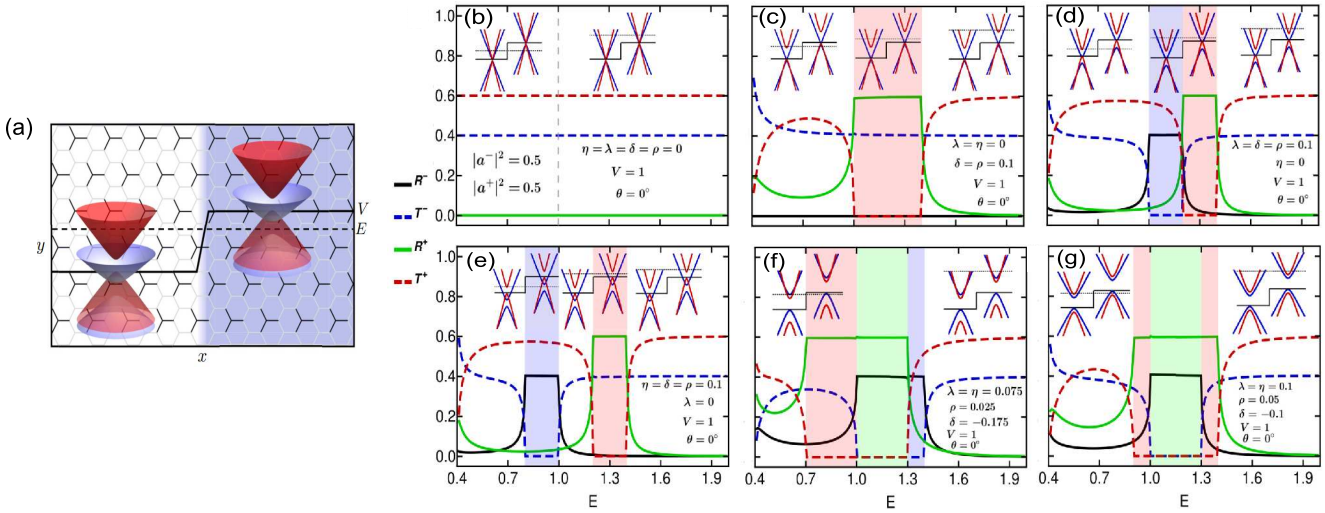


Fig. 6. (a) Schematic of a Kekulé-graphene pn junction with the potential profile shifting the energy band structures between the two regions. (b)–(g) The probabilities of reflection R^ν and transmission T^ν under normal incidence for various Kekulé-graphene pn junctions as a function of Fermi energy E with different cases. (b) Massless Dirac fermions in both valleys with the dashed-gray line separating the interband ($E < 1$) and intraband ($E > 1$) tunneling regime. (c) Chiral symmetry breaking in a single valley. (d) Quadratic band crossing point. (e) Valley–orbit coupling. (f) Crossing conduction bands. (g) Zeeman-like effect. $\nu = \pm 1$ are valley indices. The insets present the band structure of the pn junction with the Fermi energy E being represented by a dotted line. The regions of complete valley filtering are depicted by the red and blue rectangles, while the transport gap is shown as green areas. Panels (a)–(g) are reprinted figures with permission from Ref. [50]. Copyright ©2022 by the American Physical Society.

4. Valley manipulation by the Kekulé distortion

In the last section, several works are reviewed to generate the valley current or valley-polarized charge current flowing in the Kekulé-distorted graphene based hybrid junctions due to the peculiar band structure. The essence is the presence of the valley-coupling effect due to the Kekulé distortion. Numerous works were also dedicated to manipulating the valley by use of the same valley coupling effect.[30,32,34,35,40,47,53,54]

Wang *et al.*[32] studied a graphene-In_2Te_2 superlattice structure as shown in Fig. 7(a), where the graphene superlattice same as the Kekulé-distortion graphene has a valley coupling effect and thus abbreviated as GS. It was found that by adjusting the length L of the GS region the valley periodic precession can be generated in the G/GS/G structure as shown in Figs. 7(b) and 7(c). The valley precession effect is mainly attributed to the valley coupling effect in the GS. When an electron of the K (K') valley enters the GS region from the left lead, the valley-related interaction can precess the valley like a magnetic field rotating an unparallel spin, which leads to the electron exiting from the right lead in a controlled valley state, i.e., the superposition state of the two valleys (or chiral valley) depending on the concrete parameters.

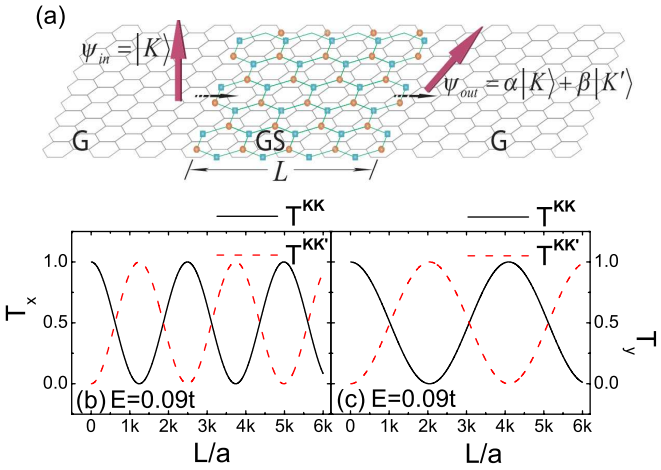


Fig. 7. (a) Schematic of a graphene/graphene-In_2Te_2/graphene structure (G/GS/G). When an electron of the K valley (wave function $\psi_{in}=|K\rangle$) enters the GS region from the left lead, it exits from the right lead and is the superposition state of the two valleys ($\psi_{out}=\alpha|K\rangle+\beta|K'\rangle$). (b) and (c) Valley-dependent transmission $T_{x(y)}^{KK(K')}$ as a function of the GS layer length L but with different site-energy modifications. The valley precession periods in panels (b) and (c) are different. The hopping energy t is set as energy unit. Panels (a)–(c) are reprinted figures with permission from Ref. [32]. Copyright ©2015 by the American Physical Society.

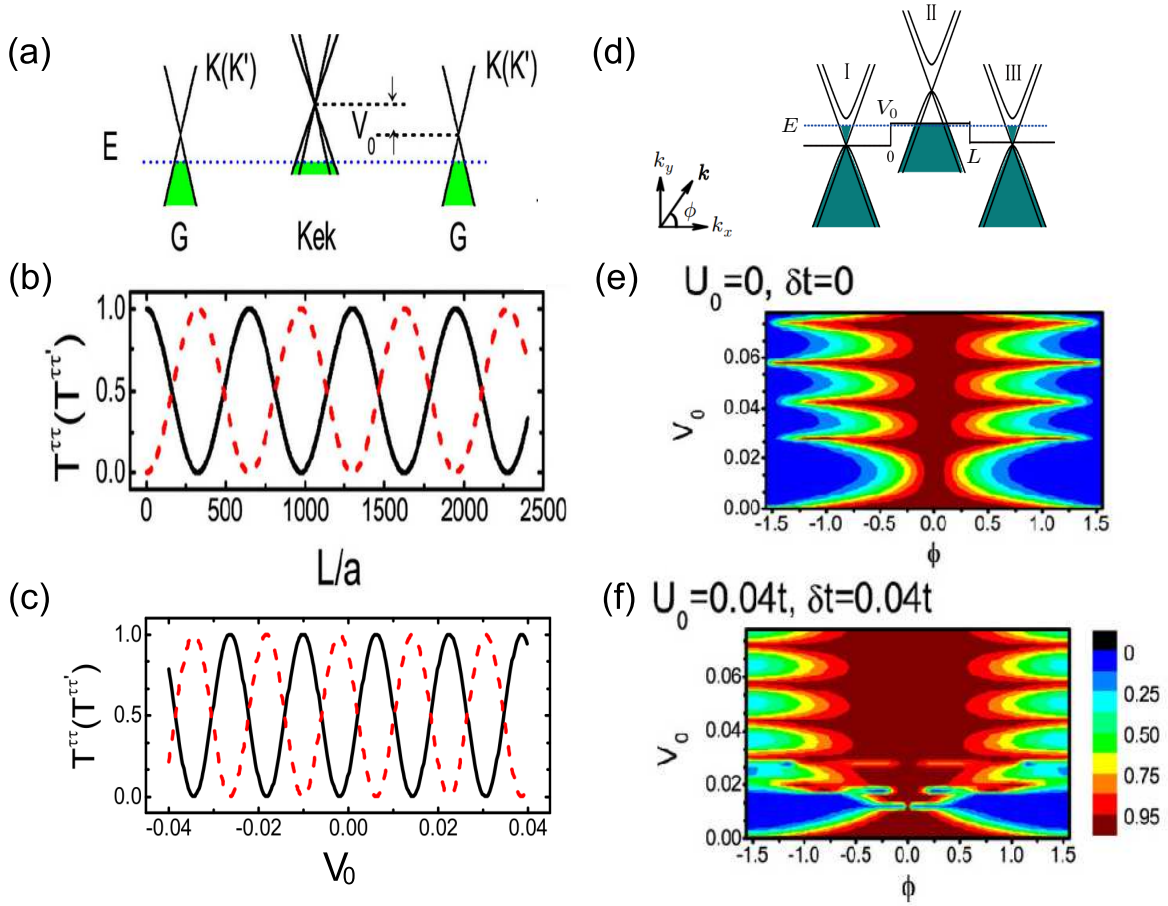


Fig. 8. (a) Schematic of a G/Y-Kek/G structure for modulating the valley degree of freedom. Transmission coefficients $T^{\tau\tau}$ ($T^{\tau\tau'}$) as a function of (b) the Y-Kek structure length L with the Fermi energy $E=-0.04t$, $V_0=0.02$, and (c) the local potential V_0 with $E=-0.01t$, $L=1200a$. (b) and (c) Other parameters are $U_0=0$, $\phi=0$ and $\delta t=0.04t$. (d) Schematic diagram of electron tunneling through a rectangular potential barrier V_0 in a Y-Kek structure with chiral symmetry breaking. Transmission coefficients T as functions of the incident angle ϕ and the local potential barrier V_0 to (e) pristine graphene and (f) Y-Kek structure with $E=0.01t$ and $L=300a$. U_0 is an extra site-energy modification of the Y-Kek structure. Panels (a)–(c), (e) and (f) are reprinted from Ref. [30]. ©2018 The Authors. Published by the American Physical Society.

The valley manipulation was also conducted by the same group in the graphene/Y-Kek/graphene structure (G/Y-Kek/G),[30] where Y-Kek superlattice structure maintains mirror symmetry as shown in Fig. 8(a). They demonstrate that the valley-related transmission coefficient $T^{\tau\tau}$ ($T^{\tau\tau'}$) exhibits periodic oscillations with the scattering region length L in Fig. 8(b). Similarly, the valley precession effect is also achievable by adjusting the gate voltage V_0 of the scattering region as shown in Fig. 8(c). The proposed method of manipulating valley freedom by adjusting gate voltage is more operable in experimental research and more convenient compared to changing the device parameters itself.

The presence of Cu vacancies in the Y-Kek structure causes a modification of the energy levels of carbon atoms with Cu vacancies, which leads to the breakdown of the mirror symmetry in the Y-Kek structure.[33] The chiral valleys are no longer the K or K' valleys in the original graphene structure. There exists only a single chiral or valley-coupling in the Y-Kek structure with appropriate parameters as shown in Fig. 2(c). Therefore, electrons in the single valley case can lead to a super Klein tunneling.[69–72] Reference [30] studied the transmission model of Fig. 8(d) and the perfection transmission can be obtained in a larger range of incident angles in Fig. 8(f) than that in the usual non-Kekulé graphene system in Fig. 8(e).

Li *et al.*[73] in a recent work studied a reversal valley precession effect in the similar Y-Kek heterostructure, which consists of the left and right Kekulé materials and a layer of strained graphene between them as shown in Fig. 9(a). Authors verified that a perfect spatial valley precession or the valley version transistor device is achievable, because the precession periodicity does not depend on the Fermi energy as well as the transverse momentum shown in Figs. 9(b)–9(e). Certainly, the precession is dependent on the local potential of Y-Kek distortion[30] and the uniform strain strength.[1,74] These two conditions are particularly useful for the valley transistor. The local strain applied onto the pristine graphene can be realized and controlled in an experiment by driving a local static potential.

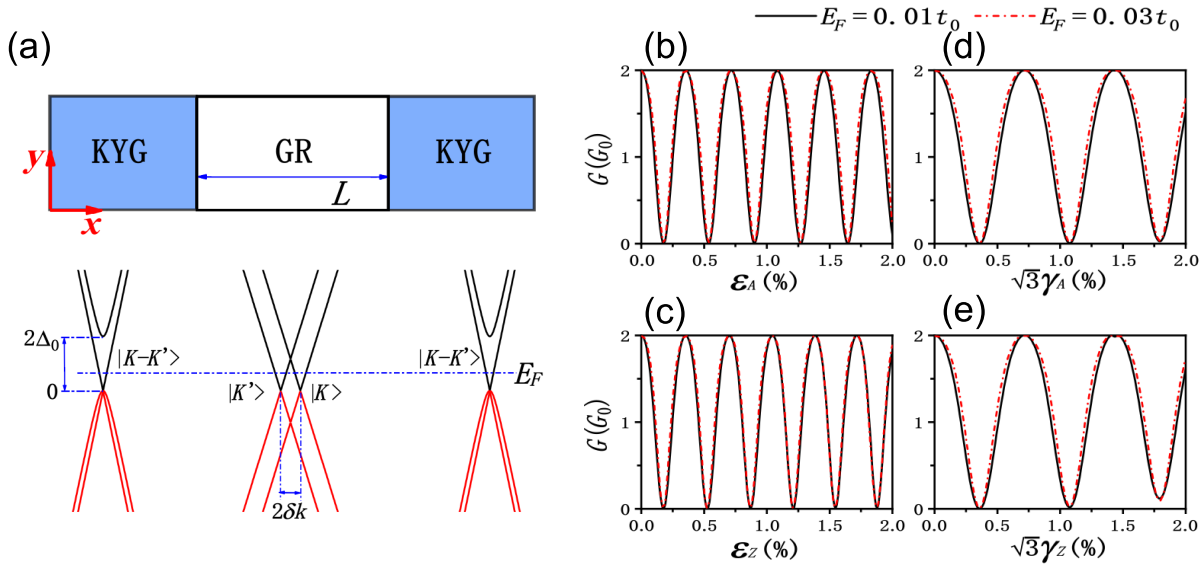


Fig. 9. (a) Top panel: schematic of the Y-Kek/graphene/Y-Kek junction (KYG/GR/KYG). Bottom panel: the band structures of the left/right Y-Kek (KYG) lead and the central strained graphene (GR) with the transverse momentum $k_y = 0$. The valley polarized electron with valley K–K' is injected into the central strained graphene region with energy E_F, and the two folded valleys K and K' of graphene are separated in the transport direction by a distance of $2\delta k$ due to strain. The conductivities of zigzag junctions vary with the strength of uniaxial strain applied in the graphene region along the (b) armchair and (c) zigzag direction. The conductivities of armchair junctions vary with the strength of shear strain applied in the graphene region along the (d) armchair and (e) zigzag directions. The on-site energy of sites A is $U_A = 0.05t_0$ and the energy splitting between the lowest conduction band and the second conduction band is $2\Delta_0 = 2U_A/3$. Panels (a)–(e) are reprinted figures with permission from Ref. [73]. Copyright ©2023 by the American Physical Society.

5. Valley-related transport due to Kekulé distortion

The valley detection is a challenging and important issue in the study of valleytronics. Currently, the detection methods mainly are based on the results of the valley transport.[75–78] For example, the valley current can be transported into the Kekulé-distortion region to generate a nonlocal voltage signal via the so-called inverse valley Hall effect.[79] In Kekulé structures, the valley polarization of currents can also be induced by introducing local charge imbalance, magnetic fields, light fields, or different impurities.

Shen *et al.*[51] constructed heterojunctions of Kekulé/normal metal/Kekulé structures as shown in Fig. 10(a) and studied the modulation of the Josephson effect by introducing non-resonant circularly polarized light in the normal non-Kekulé region. For two different Kekulé structures, the

light field excites different valley isospins in the normal region. The study shows that the non-resonant circularly polarized light causes the valleys no longer degenerate, as a result, the combined effect of the light field and the O-Kek structure fully polarize the valleys, forming a π-state superconducting Josephson junction as shown in Figs. 10(b) and 10(c). However, the Y-Kek version can only lead to a 0-state Josephson junction as shown in Figs. 10(d) and 10(e). Such a difference could be utilized to discern the valley imbalance.

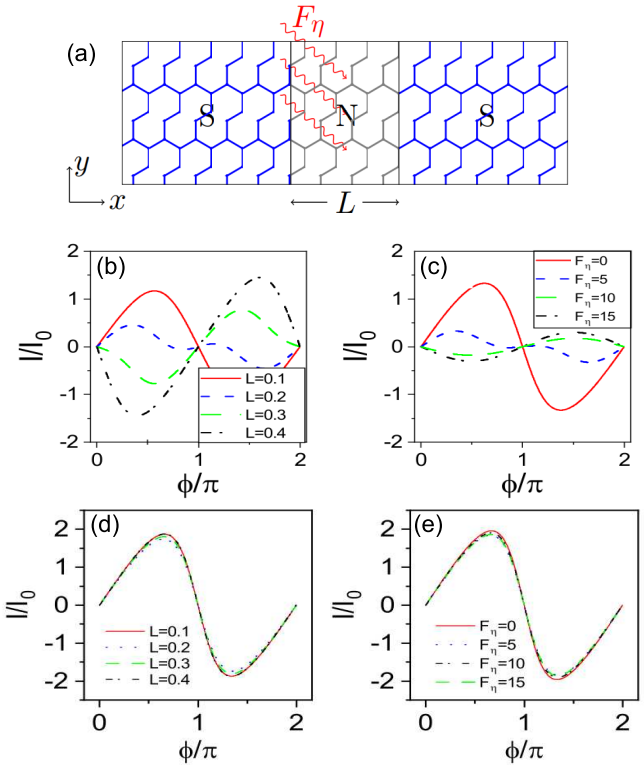


Fig. 10. (a) Schematic of a superconductor/normal metal/superconductor junction based on Kekulé structures. The illumination parameters and junction lengths are defined as F_η and L, respectively. The red wavy lines indicate the off-resonant polarized light only applied in the normal region. Josephson current in O-Kek/normal metal/O-Kek junction as a function of the phase ϕ with $C_O = 30$, (b) $F_\eta = 10$ and (c) $L = 0.1$. Josephson current in Y-Kek/normal metal/Y-Kek junction as a function of the phase ϕ with $C_Y = 0.1$, (d) $F_\eta = 10$ and (e) $L = 0.1$. (b)–(e) Other parameters are $\mu = 42$ and $T/T_c = 0.1$. $C_{O(Y)}$ represents the coupling amplitude introduced by the O-Kek (Y-Kek) bond density wave. Panels (a)–(e) are reprinted figures with permission from Ref. [51]. Copyright ©2022 by the American Physical Society.

Andrade *et al.*[52] studied the valley electron birefringence phenomenon in the original graphene structure with circularly symmetric Kekulé distortion structure as shown in Fig. 11(a). For low carrier concentrations, the locally enhanced Kekulé distortion and the local static potential should lead to skew scattering of different valley electrons in opposite directions, resulting in the valley Hall effect. This is a hallmark of the Y-Kek distortion. Authors show some characteristics of the birefringence phenomenon in Figs. 11(c) and 11(d). The negative refractive index added to the circular Kekulé graphene distortion structure can produce heart-shaped envelope interference patterns with high concentration at the tip, while the caustics and cusps of the circular lens are twice than that of the pristine graphene structure. The continuously enhanced Kekulé distortion strength can reduce the height of the central (valley-protected) peak and lead to a shift in its position in the total scattering cross section. The two new peaks correspond to quasi-bound state processes formed due to the valley mixing effect as shown in Fig. 11(b). This study shows that the valley Hall effect caused by deflection scattering can be realized and detected in Kekulé graphene structures by a four-probe experiment.

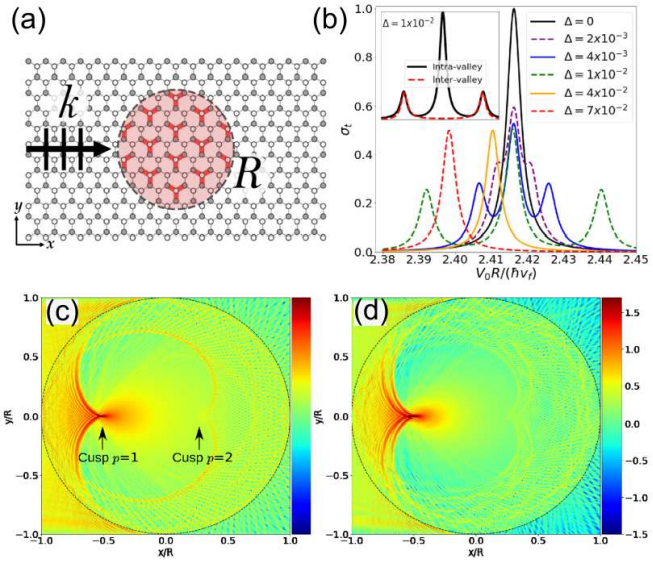


Fig. 11. (a) Schematic of a sheet of pristine graphene containing a circular Y-Kek structure of radius R (gray dashed area). Electrons in the x-direction with momentum k are incident onto a circular region of radius R with a gate potential and Y-Kek structure. (b) Total cross-section σ_t as a function of gate potential V_0 with $kR = 1.5 \times 10^{-3}$. Inset: total cross-section for intravalley $\sigma_{t,KK} + \sigma_{t,K'K'}$ and intervalley $\sigma_{t,KK'} + \sigma_{t,K'K}$ processes with Kekulé amplitude $\Delta = 0.01$. The probability density in $\log_{10}$ scale varies with space to (c) pristine graphene and (d) Y-Kek distorted graphene with $\Delta = 0.1$ in the $r < R$ region for an incoming electron flux in the x direction with valley polarization K' and $kR = 300$. The boundary between the scattering regions is indicated by the dashed line and there is a gate potential $V_0R/(\hbar v_f) = 600$ in the inner region. Panels (a)–(d) are reprinted figures with permission from Ref. [52]. Copyright ©2022 by the American Physical Society.

6. Outlook and summary

Although the valley flow like the pure spin counterpart does not have any electrical signals, the unique electronic and optical properties of the Kekulé structures can make them more useful to study valley transport even in experiment. It is hoped that the Kekulé structures can be designed as the basis of a new generation of valley-dependent electronic device. For example, the Kekulé system can be used to design and manufacture valley filters by using circularly polarized light to control valley polarization. The gap of the basis atoms opens an energy gap of the Kekulé structures, and this provides a new idea for the external electric field manipulation of qubits. The Kekulé structures can be used to detect and measure changes in valley polarization caused by external stimuli, to develop

highly sensitive sensors, and to make more efficient energy storage and processing devices as well. In short, Kekulé distorted graphene has broad application prospects in the field of valley electronics. The expected excellent performance of electronic devices based on valley electronics makes it more significant to study the Kekulé structures for potential applications in valleytronics.

At present, the study of valley transport in the Kekulé structures is mainly concentrated on the theoretical aspect. This field is still in its early stages, although experiments have successfully placed the original graphene structure on specific atomic substrates such as Li, Rb, Cs or Na to form Kekulé distorted structures.[56,80–83] However, the Kekulé distorted graphene-like materials still face some urgent problems and challenges before the practical applications. The experimental preparation of Kekulé distorted graphene materials is complex and requires high precision control, subsequently, the precise control and manipulation of valley degrees of freedom certainly have strict requirements on the device and the environment. At the same time, the holes in the distorted lattice structure can create defects that affect the electronic properties of the material due to the fabrication of the Kekulé structures, while the metal adatoms causing the same distortion effect can also weaken the mechanical properties of the material.

We have conducted an overview of the transport properties of Dirac electrons in the Kekulé-distorted graphene and focused on the Kekulé distortion effects on the valley generation, manipulation, and detection in the field of valleytronics. Numerous theoretic works are dedicated to studying the valley-related transport in the Kekulé materials as well as the energy band structure, because the Kekulé distortion can directly provide a coupling between the two opposite valleys while such valley coupling can play a significant role in the valley transport like the spin–orbit interaction in the spin transport. A few experimental works have measured the Kekulé structures in graphene, so the theoretical predictions shall make the Kekulé structures promising for fabricating the electron devices based on the valley degree of freedom.

Acknowledgment

Project supported by the National Natural Science Foundation of China (Grant Nos. 12174051 and 12304069).

References

[1] Zhai F, Zhao X F and Chang K 2010 *Phys. Rev. B* **82** 115442
[2] Rycerz A, Tworzydlo J and Beenakker C W J 2007 *Nat. Phys.* **3** 172
[3] Gunlycke D and White C T 2011 *Phys. Rev. Lett.* **106** 136806
[4] Wu Z H, Zhai F, Peeters F M, Xu H Q and Chang K 2011 *Phys. Rev. Lett.* **106** 176802
[5] Pesin D and MacDonald A H 2012 *Nat. Mater.* **11** 409
[6] Behnia K 2012 *Nat. Nanotechnol.* **7** 488
[7] Aufray B, Kara A, Vizzini S, Oughaddou H, Leandri C, Ealet B and Le Lay G 2010 *Appl. Phys. Lett.* **96** 183102
[8] Mak K F, Lee C G, Hone J, Shan J and Heinz T F 2010 *Phys. Rev. Lett.* **105** 136805
[9] Wang K T, Wang H, Xu F M, Yu Y J and Wei Y D 2023 *New J. Phys.* **25** 013019
[10] Xiao D, Liu G B, Feng W X, Xu X D and Yao W 2012 *Phys. Rev. Lett.* **108** 196802
[11] Zeng H L, Dai J F, Yao W, Xiao D and Cui X D 2012 *Nat. Nanotechnol.* **7** 490
[12] Xu X D, Yao W, Xiao D and Heinz T F 2014 *Nat. Phys.* **10** 343
[13] Guddala S, Kawaguchi Y, Komissarenko F, Kiriushechkina S, Vakulenko A, Chen K, Alu A, Menon M V and Khanikaev A B 2021 *Nat. Commun.* **12** 3746
[14] Liu Y, Lian C S, Li Y, Xu Y and Duan W 2017 *Phys. Rev. Lett.* **119** 255901
[15] Giovannetti G, Capone M, van den Brink J and Ortix C 2015 *Phys. Rev. B* **91** 121417
[16] Ezawa M 2012 *Phys. Rev. Lett.* **109** 055502
[17] Liu C C, Feng W and Yao Y 2011 *Phys. Rev. Lett.* **107** 076802
[18] Xiao D, Liu G B, Feng W, Xu X and Yao W 2012 *Phys. Rev. Lett.* **108** 196802
[19] Stegmann T and Szpak N 2016 *New J. Phys.* **18** 053016
[20] Milovanovic S P and Peeters F M 2016 *Appl. Phys. Lett.* **109** 203108
[21] Low T and Guinea F 2010 *Nano Lett.* **10** 3551
[22] Zhao X W, Li Y, Liang R D, Hu G C, Yuan X B and Ren J F 2020 *Appl. Surf. Sci.* **504** 144367
[23] Fujita T, Jalil M B A and Tan S G 2010 *Appl. Phys. Lett.* **97** 043508
[24] Garcia-Pomar J L, Cortijo A and Nieto-Vesperinas M 2008 *Phys. Rev. Lett.* **100** 236801
[25] Zhong D, Seyler K L, Linpeng X, Cheng R, Sivadas N, Huang B, Schmidgall E, Taniguchi T, Watanabe K, McGuire M A, Yao W, Xiao D, Fu K M C and Xu X D 2017 *Sci. Adv.* **3** e1603113
[26] Yao H B, Liu Y Z, Zhu M F and Zheng Y S 2015 *Europhys. Lett.* **109** 37010
[27] Wu Q P, Chang L L, Li Y Z, Liu Z F and Xiao X B 2020 *Nanoscale Res. Lett.* **15** 46
[28] Ruiz-Tijerina D A, Andrade E, Carrillo-Bastos R, Mireles F and Naumis G G 2019 *Phys. Rev. B* **100** 075431
[29] Gao P, Torrent D, Cervera F, San-Jose P, Sanchez-Dehesa J and Christensen J 2019 *Phys. Rev. Lett.* **123** 196601
[30] Wang J J, Liu S, Wang J and Liu J F 2018 *Phys. Rev. B* **98** 195436
[31] Wang J J, Liu S, Wang J and Liu J F 2020 *Phys. Rev. B* **101** 245428
[32] Wang S K and Wang J 2015 *Phys. Rev. B* **92** 075419
[33] Ren Y F, Deng X Z, Qiao Z H, Li C S, Jung J, Zeng C G, Zhang Z Y and Niu Q 2015 *Phys. Rev. B* **91** 245415
[34] Xu F M, Yu Z Z, Ren Y F, Wang B, Wei Y D and Qiao Z H 2016 *New J. Phys.* **18** 113011
[35] Wu Q P, Liu Z F, Chen A X, Xiao X B, Zhang H and Miao G X 2017 *J. Phys. Condens. Matter* **29** 395303
[36] Gutierrez C, Kim C J, Brown L, Schiros T, Nordlund D, Lochocki E B, Shen K M, Park J and Pasupathy A N 2016 *Nat. Phys.* **12** 950
[37] Lu H Z, Yao W, Xiao D and Shen S Q 2013 *Phys. Rev. Lett.* **110** 016806
[38] An X T, Xiao J, Tu M W Y, Yu H Y, Falko V I and Yao W 2017 *Phys. Rev. Lett.* **118** 096602
[39] An X T and Yao W 2020 *Phys. Rev. A* **14** 014039
[40] Gamayun O V, Ostroukh V P, Gnezdilov N V, Adagideli I and Beenakker C W J 2018 *New J. Phys.* **20** 023016
[41] Hou C Y, Chamon C and Mudry C 2007 *Phys. Rev. Lett.* **98** 186809
[42] Herrera S A and Naumis G G 2020 *Phys. Rev. B* **102** 205429
[43] Andrade E, Carrillo-Bastos R and Naumis G G 2019 *Phys. Rev. B* **99** 035411
[44] Bao C H, Zhang H Y, Zhang T, Wu X, Luo L P, Zhou S H, Li Q, Hou Y H, Yao W, Liu L W, Yu P, Li J, Duan W H, Yao H, Wang Y L and Zhou S Y 2021 *Phys. Rev. Lett.* **126** 206804
[45] Cheianov V V, Falko V I, Syljuasen O and Altshuler B L 2009 *Solid State Commun.* **149** 1499
[46] Chamon C 2000 *Phys. Rev. B* **62** 2806
[47] Zeng W and Shen R 2021 *Phys. Rev. B* **104** 075436
[48] Andrade E, Carrillo-Bastos R, Pantaleon P A and Mireles F 2020 *J. Appl. Phys.* **127** 054304
[49] Herrera S A and Naumis G G 2020 *Phys. Rev. B* **101** 205413
[50] Garcia S G, Stegmann T and Betancur-Ocampo Y 2022 *Phys. Rev. B* **105** 125139
[51] Zeng W and Shen R 2022 *Phys. Rev. B* **105** 094510

[52] Andrade E, Carrillo-Bastos R, Asmar M M and Naumis G G 2022 *Phys. Rev. B* **106** 195413
[53] Beenakker C W J, Gnezdilov N V, Dresselhaus E, Ostroukh V P, Herasymenko Y, Adagideli I and Tworzydlo J 2018 *Phys. Rev. B* **97** 241403
[54] Mojarro M A, Ibarra-Sierra V G, Sandoval-Santana J C, Carrillo-Bastos R and Naumis G G 2020 *Phys. Rev. B* **102** 165301
[55] Wu Q P, Chang L L, Li Y Z, Liu Z F and Xiao X B 2020 *Nanoscale Res. Lett.* **15** 1
[56] Virojanadara C, Watcharinyanon S, Zakharov A A and Johansson L I 2010 *Phys. Rev. B* **82** 205402
[57] Santacruz A, Iglesias P E, Carrillo-Bastos R and Mireles F 2022 *Phys. Rev. B* **105** 205405
[58] Mohammadi Y and Bahrami S 2022 *Chin. Phys. B* **31** 017305
[59] Wei Y J, Liu H L, Wang J and Liu J F 2022 *Phys. Rev. B* **106** 165419
[60] Castro Neto A H, Guinea F, Peres N M R, Novoselov K S and Geim A K 2009 *Rev. Mod. Phys.* **81** 109
[61] Sasaki K I and Saito R 2008 *Prog. Theor. Phys. Suppl.* **176** 253
[62] Eom D and Koo J Y 2020 *Nanoscale* **12** 19604
[63] Wang J and Fischer S 2014 *Phys. Rev. B* **89** 245421
[64] Iadecola T, Campbell D, Chamon C, Hou C Y, Jackiw R, Pi S Y and Kusminskiy S V 2013 *Phys. Rev. Lett.* **110** 176603
[65] Iadecola T, Neupert T and Chamon C 2014 *Phys. Rev. B* **89** 115425
[66] Xiao D, Yao W and Niu Q 2007 *Phys. Rev. Lett.* **99** 236809
[67] Beenakker C W J 2013 *Annu. Rev. Condens. Matter Phys.* **4** 113
[68] Venderbos J W F, Manzardo M, Efremov D V, van den Brink J and Ortix C 2016 *Phys. Rev. B* **93** 045428
[69] Betancur-Ocampo Y, Cordourier-Maruri G, Gupta V and de Coss R 2017 *Phys. Rev. B* **96** 024304
[70] Illes E and Nicol E J 2017 *Phys. Rev. B* **95** 235432
[71] Urban Daniel F, Bercioux D, Wimmer M and Hausler W 2011 *Phys. Rev. B* **84** 115136
[72] Shen R, Shao L B, Wang B G and Xing D Y 2010 *Phys. Rev. B* **81** 041410
[73] Li R G, Liu J F and Wang J 2023 *Phys. Rev. Appl.* **19** 024075
[74] Pereira Vitor M and Castro Neto A H 2009 *Phys. Rev. Lett.* **103** 046801
[75] Zeng H L, Dai J F, Yao W, Xiao D and Cui X 2012 *Nat. Nanotechnol.* **7** 490
[76] Shan W Y, Zhou J H and Xiao D 2015 *Phys. Rev. B* **91** 035402
[77] Wehling T O, Huber A, Lichtenstein A I and Katsnelson M I 2015 *Phys. Rev. B* **91** 041404
[78] Assili M, Haddad S and Kang W 2015 *Phys. Rev. B* **91** 115422
[79] Gorbachev R V, Song C W J, Yu G L, Kretinin A V, Withers F, Cao Y, Mishchenko A, Grigorieva I V, Novoselov K S, Levitov L S and Geim A K 2014 *Science* **346** 448
[80] Xia C, Watcharinyanon S, Zakharov A A, Yakimova R, Hultman L, Johansson L I and Virojanadara C 2012 *Phys. Rev. B* **85** 045418
[81] Watcharinyanon S, Virojanadara C and Johansson L 2011 *Surf. Sci.* **605** 1918
[82] Watcharinyanon S, Johansson L I, Xia C and Virojanadara C 2012 *J. Appl. Phys.* **111** 083711
[83] Forti S and Starke U 2014 *J. Phys. D: Appl. Phys.* **47** 094013